Check for updates

Anti-cancer activity of hierarchical ZSM-5 zeolites synthesized from rice-based waste materials†

S. K. Jesudoss,[a] J. Judith Vijaya, [iD] *[a] K. Kaviyarasu,[bc] L. John Kennedy,[d] R. Jothi Ramalingam [iD] [e] and Hamad A. Al-Lohedan[e]

Herein, organic template-free MFI-type ZSM-5 zeolites were successfully synthesized by the hydrothermal method using waste materials such as rice husk ash (RHA), rice hull ash (RHuA), and rice straw ash (RSA). The waste materials were locally obtained, precleaned, and properly heat-treated to produce a high-purity crystalline SiO_2 that was used in the synthesis of ZSM-5 zeolites under autogenous pressure in a short reaction time (5 days). The mineralogical phases, morphology, textural and thermal properties of the synthesized products were investigated by X-ray diffraction (XRD), Fourier transform infrared (FT-IR), Raman spectroscopy, high-resolution scanning electron microscopy (HR-SEM), N_2 adsorption/ desorption isotherms (BET), temperature-programmed desorption (NH_3-TPD), and thermogravimetric analysis (TGA/DTA). The as-synthesized ZSM-5 zeolites showed good crystallinity, and no amorphous material existed in the framework of the ZSM-5 zeolites after calcination and ammonium exchange processes. The characterization results prove that the high crystallinity of RHA as compared to that of the other materials (RHuA and RSA) is due to the high silica content in RHA. The transformation occurs from high-crystallinity RHA into ZSM-5 zeolite and also increases the crystallinity of zeolites. In addition, we have investigated hierarchical ZSM-5 zeolites at various concentrations for their potential cytotoxicity effect against the human lung epithelial cancer A549 cells.

1 Introduction

Zeolites have a porous crystalline aluminosilicate framework and ordered networks of micropores.[1] Generally, they are used in industry as heterogeneous catalysts for various processes such as catalysis, adsorption, separation, and ion-exchange.[2,3] They have superior catalytic activity due to the presence of zeolitic micropores with enhanced accessibility, transport, and additional larger porous structures within a single system.[4] In recent years, many ordered zeolites have been successfully developed with quintessential hierarchical porous structures within the zeolite material.[4,5]

[a]*Catalysis & Nanomaterials Research Laboratory, Department of Chemistry, Loyola College (Autonomous), Chennai 600 034, India. E-mail: jjvijaya78@gmail.com; Fax: +91-44-28175566; Tel: +91-44-28178200*

[b]*UNESCO-UNISA Africa Chair in Nanosciences/Nanotechnology Laboratories, College of Graduate Studies, University of South Africa (UNISA), Muckleneuk Ridge, P O Box 392, Pretoria, South Africa*

[c]*Nanosciences African Network (NANOAFNET), Materials Research Group (MRG), iThemba LABS-National Research Foundation (NRF), 1 Old Faure Road, P O Box 722, Somerset West, 7129, Western Cape Province, South Africa*

[d]*Materials Division, School of Advanced Sciences, Vellore Institute of Technology (VIT) University, Chennai Campus, Chennai 600 127, India*

[e]*Surfactant Research Chair, Chemistry Department, College of Science, King Saud University, Riyadh 11451, Saudi Arabia*

† Electronic supplementary information (ESI) available. See DOI: 10.1039/c7ra11763a

Pentasil-type ZSM-5 zeolites are related to the framework type of MFI [Mobile FIve]. They have generally been used in shape-selective field because of their well-defined micropores, intrinsic acidity, and high hydrothermal stability.[6–8] In general, for the synthesis of high-silica zeolites, large quantities of organic ammonium cations were used such as tetraalkylammonium ions and diamine, and they were introduced into the aluminosilicate gels for the formation of the zeolitic framework in which they served as a structure-directing agent or as a space-filling agent.[9,10] However, the organic templates needed for the synthesis are toxic and highly expensive as well as these organic species enclosed within zeolitic structures can be removed by calcination at high temperatures; this inevitably leads to both energy consumption and environmental pollution.[11,12] Therefore, organic template-free synthesis of zeolites is strongly desirable since it is more ideal, cheaper, and less toxic.[13,14]

Silica is the second most abundant element on the earth surface, which accounts for approximately 32% of the total weight of it. As a consequence, plants rooted in soil always contain a certain percentage of silicon in their tissues.[15,16] Some of the silica present in the soil surface is produced as an agricultural waste or as industrial byproducts. For example, the annual yield of rice husks, rice hulls, and rice straws was about 127 million tons in 2008.[17,18] Many investigations have shown that pure amorphous silica can be prepared from a cheap

precursor such as rice husk.[19,20] Umeda and Kondoh[21] reported the production of high-purity amorphous silica with 99.5–99.77 mass% from rice husks at 800 °C. Some successful studies have been previously reported on the production of silica from rice husk with high purity and its application for the synthesis of ZSM-5 zeolites.[22,23]

Hence, rice husk ash (RHA), rice hull ash (RHuA), rice straw ash (RSA), and the undesirable agricultural mass residues or fly ash from coal combustion in power plants can be used as the sources of silica or carbon.[24] Silica extracted from the waste materials by a suitable alkali solution has been previously reported.[25,26] The present methodology of preparation of ZSM-5 zeolite deals with the use of waste materials (RHA, RHuA, and RSA) and other aqua-based precursor materials and involves a combination of heating, leaching, and reflux treatments. It will be more advantageous as a low-cost process and beneficial for controlling the environmental pollution as well.

As per WHO (World Health Organization) survey report published in 2008, the cancer deaths have been accounted as 7.6 million (~13%) worldwide, and these deaths are predicted to reach more than 11 million in 2030.[27] Generally, lung cancer stands as the foremost cause of cancer-related deaths owing to its quick development, high occurrence, and poor diagnosis.[28] Worldwide, <15% (5 years survival rate) lung cancer-related death and health care issues have been observed in the past few years.[28,29] At present, chemotherapy has been broadly used for lung cancer treatment. However, on the other side, severe side effects have been reported for some antitumor chemotherapeutics. An A549 cell, a human pulmonary epithelial cell line, is often used as an *in vitro* model to study the lung toxicity of environmental mutagens and carcinogens. In this study, the MTT assay was used to determine the oxidative stress in A549 lung cells. The impact of hierarchical ZSM-5 zeolites against human lung epithelial cancer A549 cells has not been elucidated to date although their cytotoxicity study has been extensively investigated.

In the present study, we have demonstrated a simple and successful route for the organic template-free synthesis of ZSM-5 zeolite using waste materials (RHA, RHuA, and RSA). The synthesized products were characterized by powder X-ray diffraction (XRD) to confirm the crystallinity of the ZSM-5 zeolite structure. The characteristic vibrational and Raman bands of the hierarchical ZSM-5 zeolites were determined by Fourier transform infrared (FTIR) and Raman spectroscopy. The sample morphology was examined by high-resolution scanning electron microscopy (HR-SEM). Nitrogen adsorption and desorption measurements were carried out to find the total surface area and pore volume. Acidity and thermal stability of the samples were analyzed by temperature-programmed desorption (NH$_3$-TPD) and thermogravimetric analysis (TGA/DTA), respectively. From the abovementioned results, it can be concluded that crystalline silica extracted from RHA can be used to synthesize highly siliceous ZSM-5 zeolite as compared to that extracted from other waste materials used (RHuA and RSA). To the best of our knowledge, this is the first report on the *in vitro* cytotoxic effects of various known concentrations of hierarchical ZSM-5 zeolites against A549 human lung cancer cell lines.

2 Experimental

2.1 Materials

Silica-rich waste materials, such as RH, RHu, and RS, were obtained from the local area in the Tiruchirapalli district, Tamilnadu, India, and calcined at 700 °C for 6 h at a heating and cooling rate of 4 °C min^{-1} to obtain the corresponding ashes RHA, RHuA, and RSA. Sodium hydroxide (Qualigens fine chemicals, India, purity >97%), aluminium foil (SD Fine-Chem Ltd., India, purity >99%), ammonium nitrate (SD Fine-Chem Ltd., India, purity >98%), and deionized water (DI) were used as the starting materials for hierarchical ZSM-5 zeolite synthesis. For the investigation of cytotoxicity potential, Dulbecco's modified Eagle's medium (DMEM), glucose, ʟ-glutamine, fetal bovine serum (FBS), penicillin, streptomycin, DMSO, and HEPES were purchased from HiMedia Laboratories (Mumbai, India). A human lung adenocarcinoma epithelial (A549) cell line was purchased from the National Centre for Cell Science (NCCS, Pune, India) and preserved in the laboratory. All the chemicals were used as received without further purification.

2.2 Organic template-free synthesis of hierarchical ZSM-5 zeolites

Fig. 1 shows a schematic for the organic template-free synthesis of hierarchical ZSM-5 zeolites using waste materials (RHA, RHuA, and RSA). The typical procedure for the organic template-free synthesis of hierarchical ZSM-5 zeolite is as follows: 0.04 g of aluminium foil and 2.4 g of NaOH were dissolved in 10 mL of deionized water to obtain solution A. In addition, 9.45 g of RHA was suspended in 71 mL of deionized water to obtain solution B. After mixing the solutions A and B under stirring, aluminosilicate gel with a molar ratio of $100SiO_2 : 0.5Al_2O_3 : 20Na_2O : 3000H_2O$ was formed. The stirring was continued for 24 h at room temperature for the dispersion of the solution. The abovementioned dispersed solution was then transferred into a Teflon-lined stainless steel autoclave for crystallization at 423 K under autogenous pressure for 5 days. After this, the autoclave was cooled, and the reaction mixture was filtered, washed several times with distilled water until pH had reached 7, dried overnight at 363 K, and calcined in air at 823 K for 5 h at a heating rate of 1 °C min^{-1} and a cooling rate of 2 °C min^{-1}.

Since NaOH was used, the Na-form of the ZSM-5 zeolite was obtained, and Na-ZSM-5 zeolite was converted into the H-form by continuous ion-exchange using an excess of 1 M aqueous NH$_4$NO$_3$. The amount of the NH$_4$NO$_3$ solution added was 10 mL g^{-1} of zeolite. Then, it was filtered, washed, dried at 353 K overnight, and calcinated at 823 K for 5 h to remove the residual water, ammonia, and ammonium nitrate. The same procedure was followed for the synthesis of ZSM-5 zeolites using RHuA and RSA instead of RHA.

2.3 *In vitro* anticancer activity of the as-synthesized hierarchical ZSM-5 zeolites

2.3.1 Epithelial (A549) cell culture. *In vitro* cytotoxic activities against human lung cancer (A549) cell lines were investigated
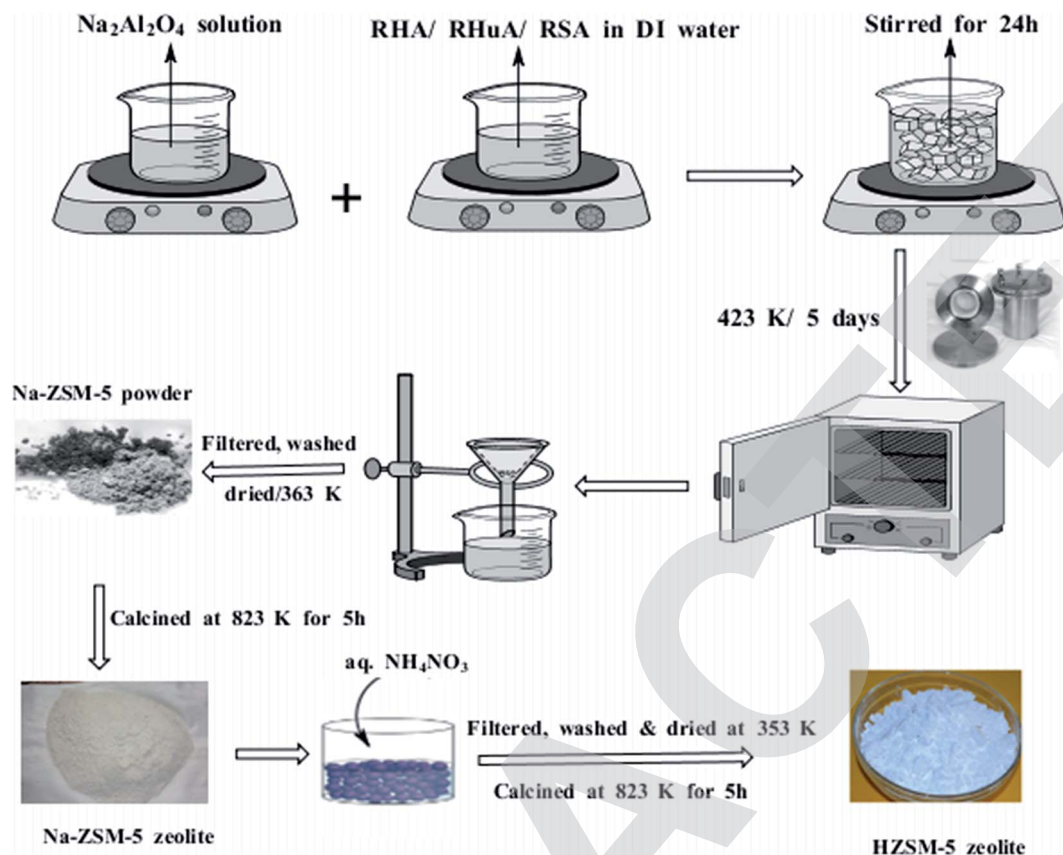
Fig. 1 Schematic for the synthesis of hierarchical ZSM-5 zeolites using waste materials (RHA, RHuA, and RSA).

in the UNESCO-UNISA Africa Chair in Nanosciences/ Nanotechnology Laboratories, University of South Africa (UNISA), South Africa. The epithelial A549 cells were cultured in a Dulbecco's modified Eagle's medium (DMEM), containing 4.5 g L^{-1} glucose, 4 mM L-glutamine, small crucial intermediate contributes with 10% fetal bovine serum (FBS), 1% penicillin/ streptomycin, and 20 mM HEPES. The cells were plated and incubated under an atmosphere of 5% CO_2 at 37 °C.

2.3.2 MTT assay. The A549 cells (1×10^5 cells per well) were coated in 96-well plates and incubated for 24 h at 37 °C under humidified atmosphere containing 95% air and 5% CO_2.[30] The hierarchical ZSM-5 zeolites were treated with the various known concentrations (23.2–1000 µg mL^{-1}) of the human epithelial cell line A549, and the control cells were treated with DMSO. Then, various concentrations of the zeolite samples were added when the cell reached confluence followed by incubation for 24 h. Finally, the samples were removed from the medium and washed with phosphate-buffered saline (pH 7.4) or DMEM without serum. After 24 h of incubation, 20 µL per well of 0.5% 3-(4,5-dimethyl-2-thiazolyl)-2,5-diphenyltetrazolium bromide (MTT) was added and incubated for 4 h. After incubation, 1 mL of DMSO was added to all the wells. In addition, more amount of DMSO was added to achieve complete solubility, and a yellow dye was changed to purple coloured formazan crystals. The absorbance was measured at 570 nm using a UV spectrophotometer. The percentage of the control is equal to the mean

absorbance value for each hierarchical ZSM-5 zeolite concentration divided by the mean value of control cells (control treated as 100%).

2.3.3 Statistical analysis. The present study data were subjected to one-way analysis of variance (ANOVA), and it was accepted at a level of $p < 0.05$. This analysis was carried out using SPSS software version 16 (SPSS Inc., Chicago, IL, USA).

2.4 Characterization

Powder X-ray diffraction (XRD) patterns were obtained using the PANalytical X'pert diffractometer with CuKα ($\lambda = 1.5418$ Å) radiation generated at 40 kV and 40 mA. The morphology of the samples was characterized using a high-resolution scanning electron microscope (HR-SEM) (JEM-6700F, JEOL, Japan). FTIR spectra were obtained *via* an FTIR spectrometer (Perkin Elmer, USA) using the dried KBr pellet technique in the range of 400–4000 cm^{-1}. Raman bands were observed using a Raman spectrophotometer (STR-250 Seki Technotron Corporation, Tokyo, Japan). Nitrogen adsorption–desorption isotherms were obtained using the Autosorb-1 analyser (Quantachrome, USA). NH_3-TPD was carried out using Micromeritics Chemisorb 2750, USA, to determine the acid sites on the hierarchical ZSM-5 zeolite materials. TGA and DTA studies were examined using thermogravimetric analytical instruments (NETZSCH STA 44950, Chennai, India), and the test was run by heating the samples up to 700 °C at a heating rate of 5 °C min^{-1} under

a high-purity nitrogen atmosphere. The cytotoxicity study was conducted using the SPSS software version 16 (SPSS Inc., Chicago, IL, USA), and the absorbance was measured at 570 nm using a UV spectrophotometer.

3 Results and discussion

3.1 X-ray diffraction studies

The powder X-ray diffraction patterns of hierarchical ZSM-5 synthesized from waste materials, such as RHA, RHuA, and RSA, are shown in Fig. 2. The synthesized materials exhibit the characteristic X-ray diffraction pattern of the MFI topology with the peaks at $2\theta = 7.9°$, 9.04°, 13.59°, 14.19°, 15.14°, 15.91°, 23.38°, 24.16°, 25.63°, and 30.18° that are associated with (101), (111), (102), (112), (131), (022), (051), (313), (323), and (062) planes, respectively. The diffraction peaks matched very well with those reported in the literature[31] and were completely indexed to the ZSM-5 zeolite structure, corresponding to the JCPDS card no. 89-1421. All the as-synthesized samples show the exact ZSM-5 XRD patterns, and no other impurity peak is observed; this indicates high purity of the products. However, the product ZSM-5 prepared from RHA shows higher crystallinity than those prepared from the other waste samples; this indicates the strong directing function of silica for zeolite crystallization. The intensities of the XRD patterns of hierarchical ZSM-5 zeolite differ with silica source although all the samples exhibit typical lines of MFI topology. The increase in line intensities is associated with the increasing silica content of the samples. Therefore, more silica is incorporated into the crystallized solid phase, thus favoring the crystallization of ZSM-5. The average crystallite size of the as-synthesized ZSM-5 zeolite was calculated using the Debye Scherrer formula (1):[32]

$$L = \frac{0.89\lambda}{\beta \cos \theta} \tag{1}$$

where L is the average crystallite size, λ is the X-ray wavelength (0.154 Å), θ is the Bragg diffraction angle, and β is the full-width at half maximum (FWHM).
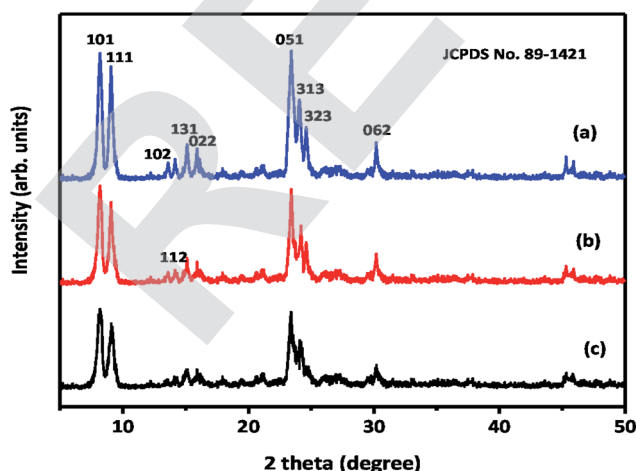

Fig. 2 X-ray diffraction patterns of hierarchical ZSM-5 zeolites: (a) ZSM-5-RHA, (b) ZSM-5-RHuA, and (c) ZSM-5-RSA.

To obtain the peak position and FWHM, the curves were fitted with two Gaussian curves for the determination of peak position and width, which belongs to the monochromatic CuKα radiation. The average crystallite sizes calculated from the diffraction peaks were found to be 27 nm for ZSM-5-RHA, 26 nm for ZSM-5-RHuA, and 23 nm for ZSM-5-RSA. The average crystallite size of the ZSM-5 zeolite differs with respect to the silica source used. The ZSM-5-RSA zeolite showed a smaller crystallite size than ZSM-RHuA and ZSM-5-RHA zeolites.

3.2 FTIR studies

The FTIR spectra of the as-synthesized organic-free hierarchical ZSM-5 zeolite samples obtained using the waste materials RHA, RHuA, and RSA are obtained in the range of 4000–400 cm^{-1} (Fig. S1†). All the samples exhibited the typical MFI framework pentasil form of ZSM-5 zeolites. The IR spectra of the synthesized samples clearly showed the characteristic absorption bands at 3644, 3459, 1614, 1224, 1087, 787, 547, and 465 cm^{-1}, which were assigned to different vibrations of tetrahedral and framework atoms in the ZSM-5 zeolite.[33,34] The characteristic band at 3644 cm^{-1} is due to the hydrogen-bonded Si–OH groups, and a broad peak around 3438 cm^{-1} is attributed to Al–OH in the zeolite framework. The band at 1614 cm^{-1} is ascribed to the OH bending vibration mode of the residual H$_2$O molecules in the zeolite voids.[35] The peaks between 400 and 1200 cm^{-1} are assigned to T–O–T framework vibrations. The bands at 1087 and 465 cm^{-1} are due to the internal bending vibration modes of (Si, Al)O$_4$ tetrahedral of ZSM-5 zeolites, which are insensitive to the framework structure.[36] Note that the vibration bands around 547 cm^{-1} indicated the presence of double 5-rings in ZSM-5.[37] The bands at 1224 and 787 cm^{-1} have been assigned to the internal asymmetric stretching vibration and external symmetric stretching of Si–O–T linkage, respectively, and they are sensitive to the ZSM-5 zeolite framework structure.

3.3 Raman spectra study

Fig. S2† displays the Raman spectrum of hierarchical ZSM-5 zeolites. Raman bands were observed at 292, 382, 442, 475, 802, 974, 1030, and 1084 cm^{-1}, respectively. A stronger band observed at 382 cm^{-1} is assigned to the v_s(Si–O–Si) bending mode of five-membered rings,[38] 292 cm^{-1} is related to the bending mode of six-membered rings, and 442 and 475 cm^{-1} are corresponding to the bending modes of the four-membered ring.[39] Concurrently, the band at 802 cm^{-1} is due to the presence of symmetric stretching, and 974, 1030, and 1084 cm^{-1} are due to the asymmetric stretching vibration modes positioned in the Raman shift range of T–O (T = Si or Al) in ZSM-5.[38–40]

3.4 HR-SEM analysis

The HR-SEM images of the synthesized ZSM-5 zeolite samples prepared from waste materials are shown in Fig. 3. Fig. 3(a–f) show the HR-SEM images of ZSM-5-RHA, ZSM-5-RHuA, and ZSM-5-RSA. The SEM images reveal that ZSM-5-RHA has a stick and sheet-like morphology (Fig. 3(a and b)), ZSM-5-RHuA possesses a stick and needle-like morphology (Fig. 3(c and d)), and ZSM-5-RSA comprises fiber-shaped arrays (Fig. 3(e and f));

moreover, their dimensions are not uniform, which is common in template-free systems.[41] In a basic medium, silica in ash materials (RHA, RHuA, and RSA) started to dissolve to form silicates. The silicates $(SiO_4)^{4-}$ and aluminate ions $(Al(OH)_4^-)$ are altered with Na^+ ions to form the channel-type hierarchical ZSM-5 zeolite, and this alkali metal ion acts as a templating agent for the formation of ZSM-5 zeolite. In the reaction system, silica was dissolved steadily during the synthesis in an alkali medium and used to enrich Si for the enhanced progress of the ZSM-5 zeolite structure. Furthermore, the inner growth of the silica and alumina molecules took place that later had led to the good arrangement of the crystalline stick-, sheet-, needle-, and fiber-like morphology for the ZSM-5 framework.

3.5 Surface area analysis

The surface area of the samples was determined from nitrogen adsorption/desorption isotherms and is shown in Fig. 4. All the

samples indicated type IV isotherms that contained a vertical uptake under $P/P_0 = 0.02$ and a hysteresis loop from $P/P_0 = 0.45$ to $P/P_0 = 1$, which was due to the coherence of both micropores and mesopores. The adhesion in the low relative pressure region indicates the presence of micropores. The ZSM-5-RHA zeolite hysteresis loop is slightly broader than that of the ZSM-5-RHuA and ZSM-5-RSA zeolites; this confirms the formation of additional mesopores in the ZSM-5-RHA zeolite. In the hierarchical ZSM-5 zeolite catalyst, the development of mesoporosity is usually due to the intercrystalline voids created by the accumulated nanoparticles.[42,43] These results indicate that the additional mesoporosity is generated without the destruction of microporosity. The parameters including the BET surface area, micropore surface area, mesopore surface area, total pore volume, micropore volume, and mesopore volume are obtained from the BET equation and the t-plot method (Table 1). The results indicate that the surface areas and pore
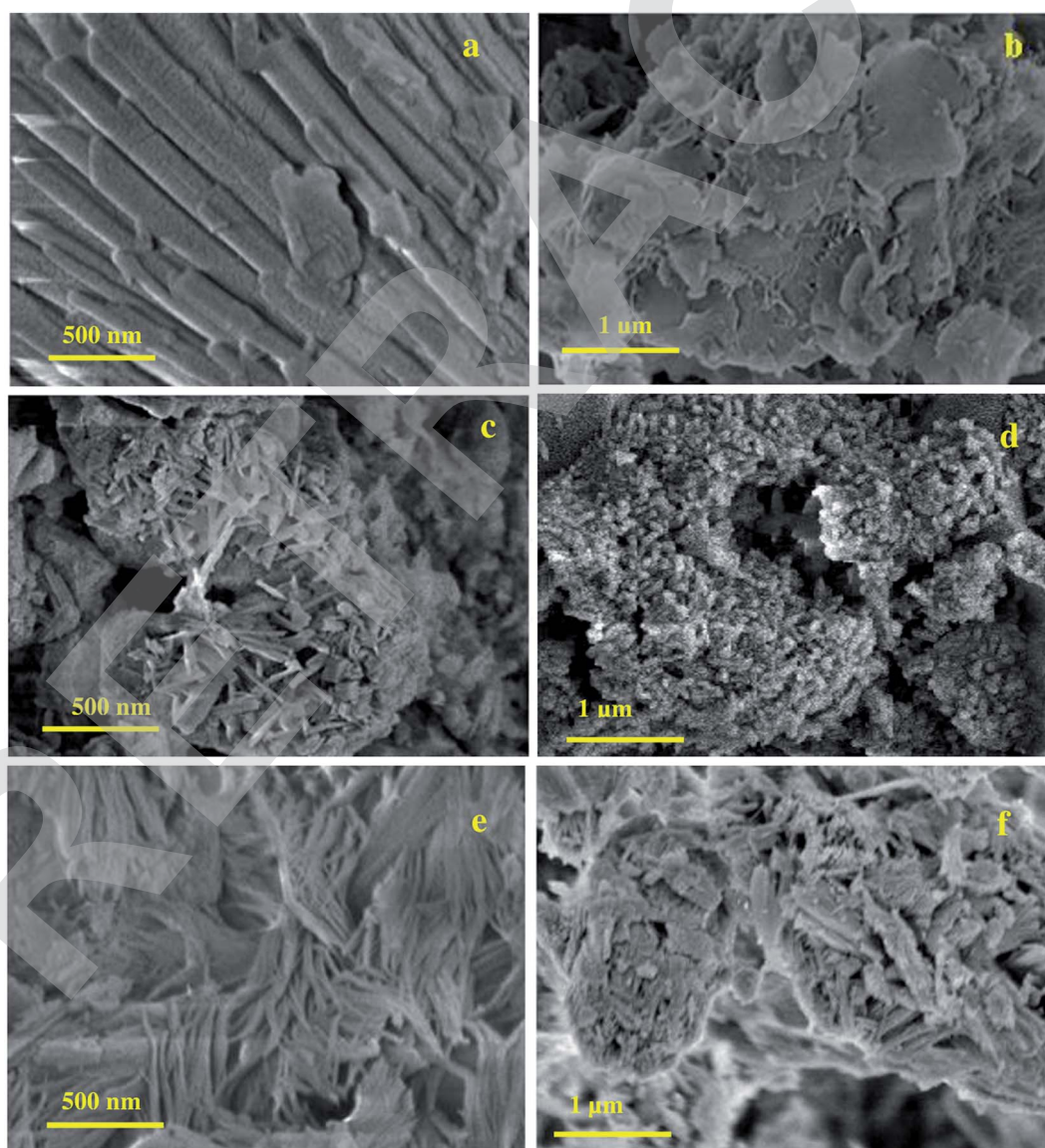

Fig. 3 HR-SEM images of hierarchical ZSM-5 zeolites morphology (a and b) ZSM-5-RHA, (c and d) ZSM-5-RHuA, and (e and f) ZSM-5-RSA.
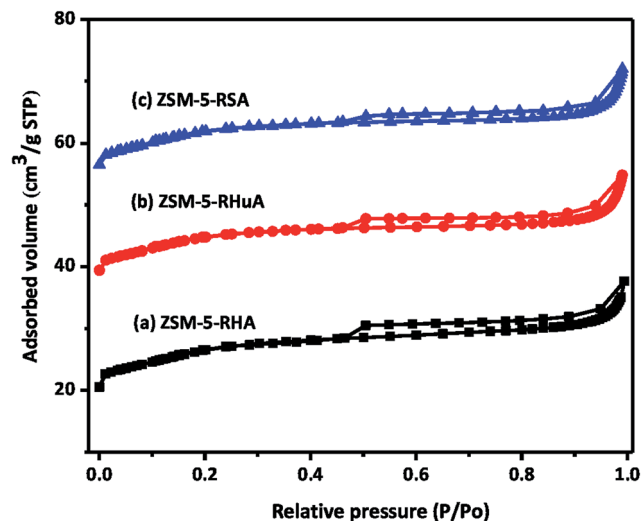
Fig. 4 N$_2$ adsorption/desorption isotherms of as-synthesized hierarchical ZSM-5 zeolites (a) ZSM-5-RHA, (b) ZSM-5-RHuA, and (c) ZSM-5-RSA.

Fig. 5 PSD of hierarchical ZSM-5 zeolites: (a) ZSM-5-RHA, (b) ZSM-5-RHuA, and (c) ZSM-5-RSA.

volumes increase with an increase in the silica content of the samples. As can be seen, more silica content of the ZSM-5-RHA zeolite helps in increasing the microporosity, thus giving rise to a final product with a specific surface area of 95 m^2 g^{-1} (micropore surface area, 68 m^2 g^{-1} and mesopore surface area 27 m^2 g^{-1}) and a total pore volume of 0.0582 cm^3 g^{-1} (micropore volume, 0.0278 cm^3 g^{-1} and mesopore volume 0.0304 cm^3 g^{-1}) as compared to the case of ZSM-5-RHuA and ZSM-5-RSA zeolite catalysts.

The pore size distributions (PSD) of ZSM-5-RHA, ZSM-5-RHuA, and ZSM-5-RSA samples are shown in Fig. 5. The plots were generated from the BJH desorption isotherm, and the mean pore diameter of ZSM-RHA (1.8 nm) was larger than that of ZSM-5-RHuA (1.74 nm) and ZSM-5-RSA (1.63 nm); this indicated the formation of additional mesopores. Thus, the isotherm results confirmed the formation of the hierarchical ZSM-5 zeolites. These hierarchical structures play a vital role in various catalytic and biomedical applications.[44–46]

3.6 Temperature-programmed desorption analysis

Temperature-programmed desorption of ammonia (NH$_3$-TPD) was carried out to depict the acidic nature of the hierarchical ZSM-5 zeolite samples, as illustrated in Fig. S3.† As shown in the figure, it has two desorption peaks at 200 °C as a low-temperature peak and at 400 °C as a high-temperature peak.
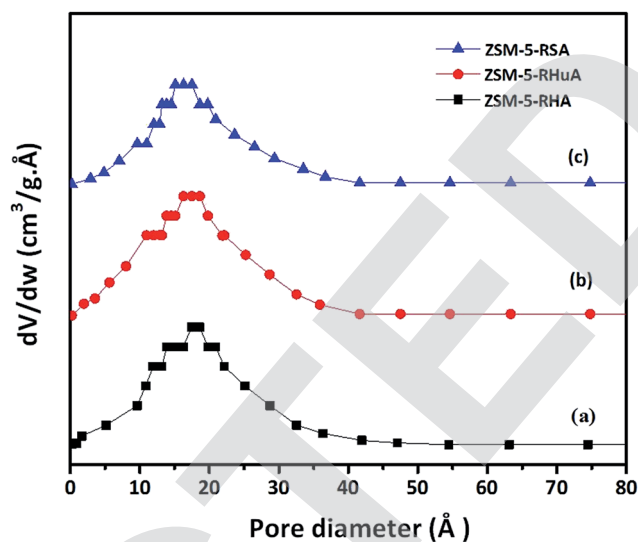
The peaks at 200 °C are owing to the weak acidic sites, and the peak at 400 °C is ascribed to the strong acid sites (Brönsted and Lewis acid sites).[47] The figure of the ammonia desorption peak of all the hierarchical ZSM-5 zeolite samples is extremely similar. The peak intensity of ZSM-5-RHA zeolite is higher than that of the ZSM-5-RHuA and ZSM-5-RSA zeolite since the hierarchical ZSM-5-RHuA and ZSM-5-RSA zeolite samples have weaker acid strength owing to the tiny quantity of aluminium built in the zeolite structure, and amorphous aluminosilicates of the macropore walls are obtained. The obtained TPD reports are in accordance with the XRD pattern results.

3.7 Thermogravimetric analysis

TGA and DTA studies were performed for the as-prepared hierarchical ZSM-5 zeolites to evaluate the weight loss as a function of temperature. The TGA curves of the hierarchical ZSM-5 zeolites show (Fig. S4a†) the respective mass losses as 8.25% (ZSM-5-RHA), 7.70% (ZSM-5-RHuA), and 6.95% (ZSM-5-RSA) up to 200 °C, which were ascribed to the removal of water from the zeolite molecules,[47] and the next significant mass losses at 250–550 °C were due to the elimination of inner water molecules or a solid-to-solid phase transition in the ZSM-5 pores.[48] The weight losses occurring at high temperatures of 550–700 °C can be attributed to the blazing of impurities, loss of humidity, and elimination of inner water molecules in the zeolite framework. The complete mass loss of

Table 1 Textural parameters of hierarchical ZSM-5-RHA, ZSM-5-RHuA, and ZSM-5-RSA zeolites

Catalyst	S_{BET} (m^2 g^{-1})	S_{micro}[a] (m^2 g^{-1})	S_{meso} (m^2 g^{-1})	V_{total} (cm^3 g^{-1})	V_{micro} (cm^3 g^{-1})	V_{meso}[b] (cm^3 g^{-1})
ZSM-5-RHA	95	68	27	0.0582	0.0278	0.0304
ZSM-5-RHuA	94	67	27	0.0560	0.0269	0.0291
ZSM-5-RSA	86	61	25	0.0534	0.0254	0.028

[a] Measured by the t-plot method. [b] $V_{meso} = V_{total} - V_{micro}$.

Table 2 MTT assay measurement of various percentages of cell deaths for different concentrations of hierarchical ZSM-5 zeolites prepared using diverse waste–based rice materials

	MTT assay			
		Cell deaths (%)		
S. no.	Concentration ($\mu g\ mL^{-1}$)	ZSM-5-RHA	ZSM-5-RHuA	ZSM-5-RSA
1	1000	77.8	72.5	67.9
2	500	64.5	61.4	56.8
3	250	55.2	50.5	46.0
4	175	41.4	36.5	32.2
5	89.5	36.5	31.7	27.2
6	51.3	21.9	17.5	14.7
7	23.2	04.0	02.5	01.6

the ZSM-5-RHA catalyst is superior to that of ZSM-5-RHuA and ZSM-5-RSA catalysts. The DTA curves (Fig. S4b†) of the hierarchical ZSM-5 catalysts (ZSM-5-RHA, ZSM-5-RHuA, and ZSM-5-RSA) show a sharp and strong endothermic peak close to 90 °C beside three small endothermic peaks at approximately 38, 150, and 220 °C. The endothermic peaks indicated the removal of physisorbed water and interior water molecules in the zeolite structure. The thermogravimetric analysis results concluded that all the hierarchical ZSM-5 catalysts were more stable at high temperatures.

3.8 *In vitro* cytotoxicity effects of hierarchical ZSM-5 zeolites

The effects of hierarchical ZSM-5 zeolites on the A549 epithelial cell membrane have been investigated by an *in vitro* model, which is known to be a more appropriate method to understand the lung epithelium response to ZSM-5. For this purpose, hierarchical ZSM-5 zeolites (ZSM-5-RHA, ZSM-5-RHuA, and ZSM-5-RSA) have been treated with various known concentrations (1000, 500, 250, 175, 89.5, 51.3, and 23.2 $\mu g\ mL^{-1}$) of the human lung epithelial cell line A549, which is known to contain adenocarcinoma human alveolar basal epithelial cells, and the cytotoxicity for each concentration level has been measured using the MTT assay. Our results indicate that the A549 cell line undergoes interactions with ZSM-5 zeolites by endocytotic mechanisms. The cells were plated and incubated under an atmosphere of 5% CO_2 at 37 °C. Then, zeolite samples were added when the cell reached confluence followed by incubation for 24 h. Finally, the samples were removed from the medium and washed with phosphate-buffered saline (pH 7.4) or DMEM without serum. Then, 20 μL per well of 0.5% 3-(4,5-dimethyl-2-thiazolyl)-2,5-diphenyltetrazolium bromide (MTT) was added and incubated for 4 h. After incubation, 1 mL of DMSO was added to all the wells. The absorbance was measured at 570 nm using a UV spectrophotometer and DMSO as the blank.[49] The cytotoxicity was determined using 50% growth inhibition of the cancer cells (IC50 value), and from the formula given below, the drug concentration was determined distinctly. The % cell viability was calculated using the following formula (2):

$$\% \text{ Cell viability} = \text{OD sample mean/OD control mean} \times 100\%$$
(2)

A graph is plotted with the percentage cell viability in the *y*-axis and various concentrations of the ZSM-5 zeolite samples in the *x*-axis. Our results indicated that at higher concentrations, there was a direct dose–response relationship of the samples with the tested cells. Table 2 displays the various percentages of cell death upon treatment with different concentrations of the hierarchical ZSM-5 zeolites. It is obviously observed from Table 2 that the ZSM-RHA values indicate better activity of other rice waste-based hierarchical ZSM-5 materials. As a rule, the cell death percentage value should increase with an increase in the concentration of zeolite particles, and the percentage should depend on the dosage level. Moreover, higher concentrations (1000 $\mu g\ mL^{-1}$) of hierarchical ZSM-5 zeolites of 77.8% (ZSM-RHA), 72.5% (ZSM-5-RHuA), and 67.9% (ZSM-5-RSA) of cell deaths were observed. Thus, 175 $\mu g\ mL^{-1}$ concentrations of hierarchical ZSM-5 catalysts are adequate to retard 41.4% (ZSM-RHA), 36.5% (ZSM-5-RHuA), and 32.2% (ZSM-5-RSA) of A549 lung cancer cells. The graph in Fig. 6 shows the different percentages of cell viability against varied concentrations of the hierarchical ZSM-5-RHA, ZSM-5-RHuA, and ZSM-5-RSA zeolites. Accordingly, low quantities of cell viability, such as 22.2% (ZSM-5-RHA), 27.5% (ZSM-5-RHuA), and 32.1% (ZSM-5-RSA), were observed at maximum concentrations (1000 $\mu g\ mL^{-1}$), and they increased gradually to higher quantities of cell viability, such as 96.0% (ZSM-5-RHA), 97.5% (ZSM-5-RHuA), and 98.4% (ZSM-5-RSA), at a low concentration (23.2 $\mu g\ mL^{-1}$), which was observed towards A549 epithelial cell lines treated with hierarchical ZSM-5 zeolites. The abovementioned results indicate that the ZSM-5 zeolites have a significant role in damaging the A549 human lung epithelial cells and agree very well with that reported previously.[50] The enhanced cytotoxicity is fundamentally owing to strong affinity of these zeolites towards biological macromolecules and their easy permeability to the cellular barriers, which results in the release of reactive oxygen species (ROS) that cause damage to the cellular components through intracellular oxidative stress.[51] Cell viability test
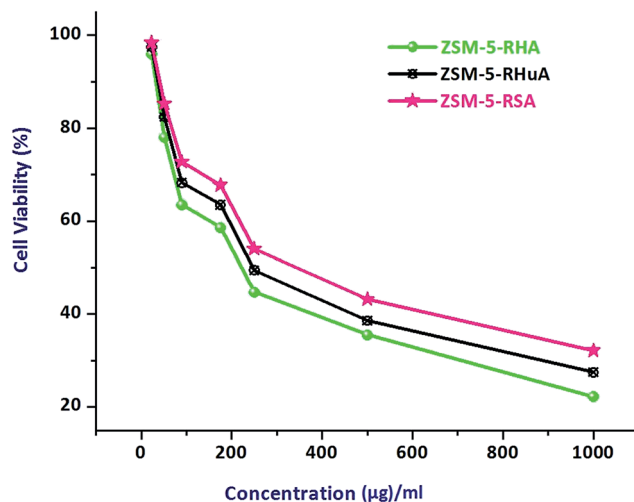

Fig. 6 MTT assay measurement on different percentages of cell viability against varied concentrations of hierarchical ZSM-5-RHA, ZSM-5-RHuA, and ZSM-5-RSA zeolites.

obviously explains the cellular response to a toxicant and implicates that the induced cytotoxicity of zeolite nanoparticles is utterly based on their size, shape, and surface chemistry.[52] In Fig. 7, the cell morphology of A549 human lung cancer cell lines treated with various concentrations of hierarchical ZSM-5-RHA zeolites is displayed. It revealed that the hierarchical ZSM-5-RHA zeolites showed superior cytotoxicity in cell lines than other zeolites, and the control cell displayed a surface with a regular and smooth nature. The cells treated with zeolite samples showed morphological changes, which occurred due to the swelling and breaking of cells. Therefore, the ZSM-5-RHA zeolite particles released into the cells can act as an exogenous carrier and ultimately results in oxidative stress. The resultant effective cytotoxic effect of hierarchical ZSM-5 zeolites discloses that a higher concentration of zeolite particles induces a significant number of reactive oxygen species through mitochondrial dysfunction in both direct and indirect manner and hence results in cell death. The schematic for the cytotoxicity effect of

hierarchical ZSM-5 zeolite nanoparticles against A549 human lung epithelial cell lines is shown in Fig. 8. The different mechanisms proposed were based on the metal ion zeolite particles released that depended on the activation of calcium and stress-inducible signalling cascades, which interfered with DNA repair pathways and cause epigenetic changes.[53,54] During metabolic processes, the continuous generation of ROS induces oxidative stress, which can lead to the DNA breaking, apoptosis, damage of cell membranes, inactivation of enzymes, and damage of genetic material and other vital cell components.[55] Oxidative stress developed from the electron transfer in the reactive oxygen species produces more free radicals such as $^{\bullet}OH$, $H_2O_2^{\bullet}$, and $O^{2\bullet-}$, and it performs a crucial role in the increase of chronic and degenerative diseases such as cancer, aging, arthritis, cardiovascular, neurodegenerative diseases, and autoimmune disorder.[56,57] Hence, this study identifies the ZSM-5-RHA zeolite as a potential biomaterial with an enhanced cytotoxicity effect, which occurs through the generation of ROS and oxidative stress,
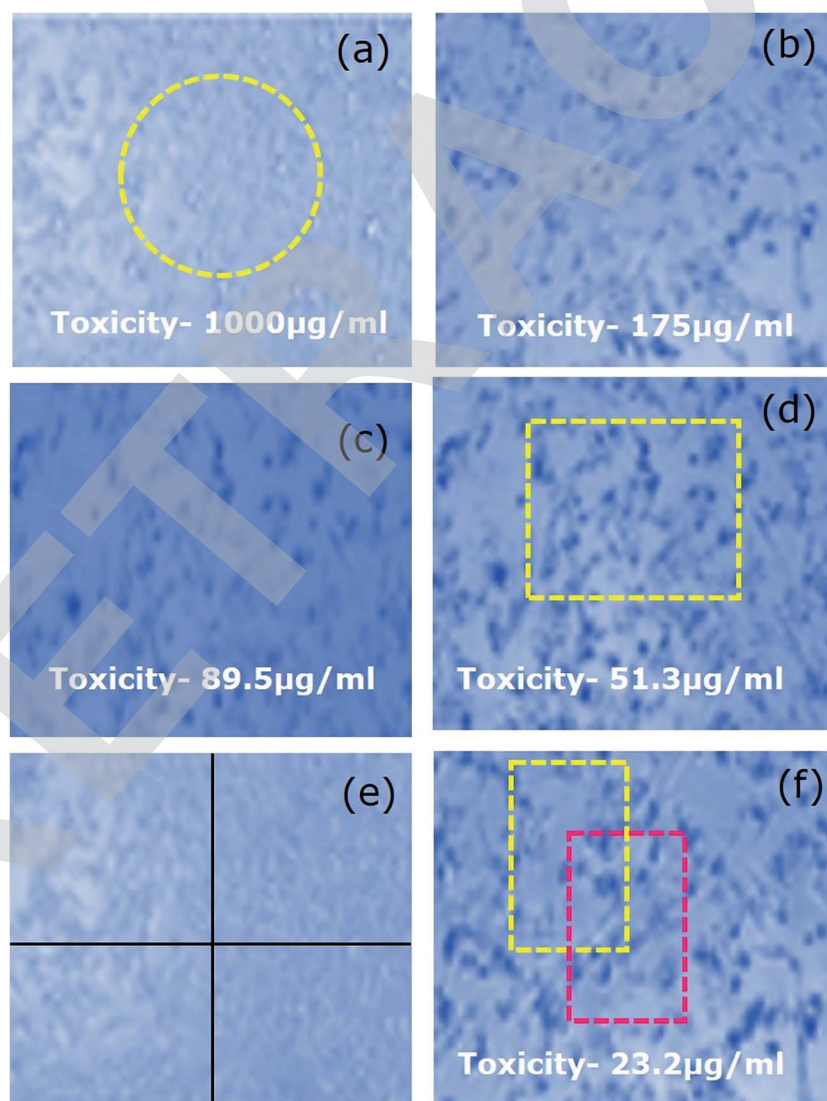

Fig. 7 (a–f) Effect on A549 (human lung epithelial cells lines) morphology upon treatment with various concentrations of hierarchical ZSM-5-RHA zeolites.
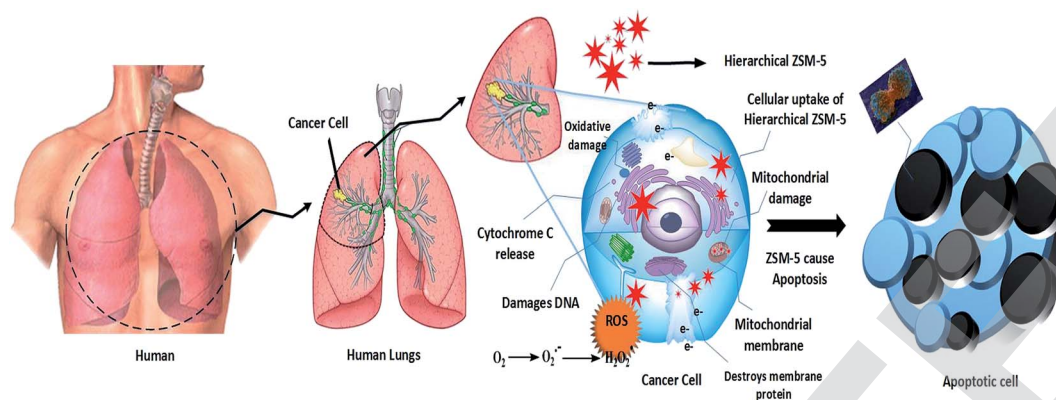
Fig. 8 Schematic of cytotoxicity effect of hierarchical ZSM-5 zeolites against A549 human lung epithelial cell lines.

against A549 human lung epithelial cell lines. The results indicate that the hierarchical ZSM-5 zeolites synthesized from rice-based waste materials such as rice husk ash, rice hulls ash, and rice straw ash have a superior anti-cancer activity against human lung cancer (A549) cell line and thereby potential applications for cancer therapy.

4 Conclusion

We successfully synthesized hierarchical ZSM-5 zeolites using rice-based waste materials, such as RHA, RHuA, and RSA, as a silica source without using any organic templates, and the samples were characterized using XRD, FTIR and Raman spectroscopy, HR-SEM, N_2 adsorption/desorption isotherms, NH_3-TPD, and TGA/DTA analysis. This method is inexpensive and does not involve the use of any costly organic templates. It is an eco-friendly and easy method that does not require template removal and needs less synthesis time. The agricultural waste material is converted into high value-added products. Herein, the superior anti-cancer activity of hierarchical ZSM-5 zeolites at various known concentrations against A549 human lung epithelial cell lines was investigated for the first time.

Conflicts of interest

The authors have declared that they have no conflicts of interests.

Acknowledgements

References

1 D. W. Breck, *Zeolite Molecular Sieves, Structure, Chemistry and Use*, John Wiley & Sons, New York, London, Sydney, Toronto, 1974.

2 M. Khatamin, A. A. Khandar, M. Haghighi, M. Ghadiri and M. Darbandi, *Powder Technol.*, 2010, **203**, 503–509.

3 T. Motsi, N. A. Rowson and M. J. H. Simmons, *Int. J. Miner. Process.*, 2011, **101**, 42–49.

4 S. Lopez-Orozco, A. Inayat, A. Schwab, T. Selvam and W. Schwieger, *Adv. Mater.*, 2011, **23**, 2602–2615.

5 J. Pérez-Ramírez, C. H. Christensen, K. Egeblad, C. H. Christensen and J. C. Groen, *Chem. Soc. Rev.*, 2008, **37**, 2530–2542.

6 Z. Gabelica, E. G. Derouane and N. Blom, Factors affecting the synthesis of pentasil zeolites, in *Catalytic Materials: Relationship between Structure and Reactivity*, ed. T. E. Whyte Jr, R. A. Dalla Betta, E. G. Derouane and R. T. K. Baker, ACS Symposium Series, American Chemical Society, Washington, DC, 1984, vol. 248, pp. 219–236.

7 L. Zhao, B. Shen, J. Gao and C. Xu, *J. Catal.*, 2008, **258**, 228–234.

8 Y. Wang, S. Fan, J. Zhang and T. S. Zhao, *Cryst. Res. Technol.*, 2015, **50**, 522–527.

9 C. S. Cundy and P. A. Cox, *Microporous Mesoporous Mater.*, 2005, **82**, 1–78.

10 S. Soltanali, R. Halladj, A. Rashidi and M. Bazmi, *Cryst. Res. Technol.*, 2014, **49**, 366–375.

11 N. Ren, J. Bronic, T. A. Jelic, A. Palcic and B. Subotic, *Cryst. Growth Des.*, 2012, **12**, 1736–1745.

12 R. Chal, C. Gerardin, M. Bulut and S. V. Donk, *ChemCatChem*, 2011, **3**, 67–81.

13 R. Lai and G. R. Gavalas, *Microporous Mesoporous Mater.*, 2000, **38**, 239–245.

14 N. L. Chauhan, J. Das, R. V. Jasra, Z. V. P. Murthy and P. A. Parikh, *Cryst. Res. Technol.*, 2012, **47**, 746–753.

15 H. Chen, F. Wang, C. Zhang, Y. Shi, G. Jin and S. Yuan, *J. Non-Cryst. Solids*, 2010, **356**, 2781–2785.

16 U. Kalapathy, A. Proctor and J. Shultz, *Bioresour. Technol.*, 2002, **85**, 285–289.

17 FAO (Food and Agriculture Organization of the United Nations), the State of Food and Agriculture Asia and the Pacific Region, Bangkok, Regional Office for Asia and the Pacific, 2008.

18 X. Chen, S. Lv, P. Zhang, L. Zhang and Y. Ye, *J. Therm. Anal. Calorim.*, 2011, **104**, 1055–1062.

19 T. Li and T. Wang, *Mater. Chem. Phys.*, 2008, **112**, 398–401.

20 L. Sun and K. Gong, *Ind. Eng. Chem. Res.*, 2001, **40**, 5861–5877.

21 J. Umeda and K. Kondoh, *Ind. Crops Prod.*, 2010, **32**, 539–544.

22 Y. Liu, Y. Guo, W. Gao, Z. Wang, Y. Ma and Z. Wang, *J. Cleaner Prod.*, 2012, **32**, 204–209.

23 P. Hemalatha, M. Bhagiyalakshmi, M. Ganesh, M. Palanichamy, V. Murugesan and H. T. Jang, *J. Ind. Eng. Chem.*, 2012, **18**, 260–265.

24 G. Chandrasekar and W.-S. Ahn, *J. Non-Cryst. Solids*, 2008, **354**, 4027–4030.

25 Z. Ramli and H. Bahruji, *Malaysian Journal of Chemistry*, 2003, **5**, 48–55.

26 H. Hamdan, M. N. M. Muhid, S. Endud, E. Listiorini and Z. Ramli, *J. Non-Cryst. Solids*, 1997, **211**, 126–131.

27 WHO Library Cataloguing-in-Publication Data, *World Health Statistics, 1. Health Status Indicators, 2. World Health, 3. Health Services-Statistics, 4. Mortality, 5. Morbidity, 6. Life Expectancy, 7. Demography, 8. Statistics, I. World Health Organization*, WHO Press, Switzerland, 2010, ISBN 978 92 4 156398 7, (NLM classification: WA 900.1).

28 Y. Wei, Y. Xu, X. Han, Y. Qi, L. Xu, Y. Xu, L. Yin, H. Sun, K. Liu and J. Peng, *Food Chem. Toxicol.*, 2013, **59**, 118–128.

29 J. A. Vaz, G. M. Almeida, I. C. F. R. Ferreira, A. Martins and M. H. Vasconcelos, *Food Chem.*, 2012, **132**, 482–486.

30 P. Palaniappan, G. Sathiskumar and R. Sankar, *Spectrochim. Acta, Part A*, 2015, **138**, 885–890.

31 T. A. J. Hardenberg, L. Mertens, P. Mesman, H. C. Muller and C. P. Nicolaides, *Zeolites*, 1992, **12**, 685–689.

32 A. Becheri, M. Durr, P. L. Nostro and P. Baglioni, *J. Nanopart. Res.*, 2008, **10**, 679–689.

33 V. Sundraramurthy and N. Lingappan, *J. Mol. Catal. A: Chem.*, 2000, **160**, 367–375.

34 M. M. Mohamed, I. O. Ali and N. A. Eissa, *Microporous Mesoporous Mater.*, 2005, **87**, 93–102.

35 M. M. Mohamed, F. I. Zidan and M. Thabet, *Microporous Mesoporous Mater.*, 2008, **108**, 193–203.

36 K. F. M. G. J. Scholle, W. S. Veeman, P. Frenken and G. P. M. V. D. Velden, *Appl. Catal.*, 1985, **17**, 233–259.

37 I. O. Ali, *Mater. Sci. Eng., A*, 2007, **459**, 294–302.

38 G. T. M. Kadja, V. A. Fabiani, M. H. Aziz, A. T. N. Fajar, A. Prasetyo, V. Suendo, E.-P. Ng and R. R. Mukti, *Adv. Powder Technol.*, 2017, **28**, 443–452.

39 Y. Yu, G. Xiong, C. Li and F.-S. Xiao, *Microporous Mesoporous Mater.*, 2001, **46**, 23–34.

40 P. K. Dutta and M. Puri, *J. Phys. Chem.*, 1987, **91**, 4329–4333.

41 R. K. Vempati, R. Borade, R. S. Hegde and S. Komarneni, *Microporous Mesoporous Mater.*, 2006, **93**, 134–140.

42 G. Majano, A. Darwiche, S. Mintova and V. Valtchev, *Ind. Eng. Chem. Res.*, 2009, **48**, 7084–7091.

43 N. Viswanadham, R. Kamble, M. Sing, M. Kumar and G. M. Dhar, *Catal. Today*, 2009, **141**, 182–186.

44 N. Chu, J. Yang, C. Li, J. Cui, Q. Zhao, X. Yin, J. Lu and J. Wang, *Microporous Mesoporous Mater.*, 2009, **118**, 169–175.

45 S. E. Lehman and S. C. Larsen, *Environ. Sci.: Nano*, 2014, **1**, 200–213.

46 C. Fernandez, I. Stan, J. P. Gilson, K. Thomas, A. Vicente, A. Bonilla and J. P. Ramirez, *Chemistry*, 2010, **16**, 6224–6233.

47 S. Narayanan, J. J. Vijaya, S. Sivasanker, L. J. Kennedy and S. K. Jesudoss, *Powder Technol.*, 2015, **274**, 338–348.

48 C. M. Magdalane, K. Kaviyarasu, J. J. Vijaya, B. Siddhardha and B. Jeyaraj, *J. Photochem. Photobiol., B*, 2016, **163**, 77–86.

49 K. Kaviyarasu, N. Geetha, K. Kanimozhi, C. M. Magdalane, S. Sivaranjani, A. Ayeshamariam, J. Kennedy and M. Maaza, *Mater. Sci. Eng., C*, 2017, **74**, 325–333.

50 M. Samiei, N. Ghasemi, N. Asl-Aminabadi, B. Divband, Y. Golparvar-Dashti and S. Shirazi, *Dent. Clin. Exp. J.*, 2017, **9**, e356–e360.

51 M. A. F. Molina, E. M. Gamboa, C. A. S. Rivera, R. A. G. Flores, P. Z. Benavides, P. C. Tello, J. M. A. González, D. F. M. Hernández, R. S. T. Guerra and C. R. Padilla, *J. Exp. Clin. Cancer Res.*, 2010, **29**, 148.

52 A. Nel, T. Xia, L. Madler and N. Li, *Science*, 2006, **311**, 622–627.

53 H. Sun, M. Shamy and M. Costa, *Genes*, 2013, **4**, 583–595.

54 H. Chen, N. C. Giri, R. Zhang, K. Yamane, Y. Zhang, M. Maroney and M. Costa, *J. Biol. Chem.*, 2010, **285**, 7374–7383.

55 H. Zhan, T. Suzuki, K. Aizawa, K. Miyagawa and R. Nagai, *J. Biol. Chem.*, 2010, **285**, 29662–29670.

56 A. Aranda, L. Sequedo, L. Tolosa, G. Quintas, E. Burello, J. V. Castell and L. Gombau, *Toxicol. In Vitro*, 2013, **27**, 954–963.

57 A. P. Lian, H. Hua and P. H. Chuong, *Int. J. Biol. Sci.*, 2008, **4**, 89–96.